Analysis of strong refractive effect within ^{11}Li projectile structure

Kassem O. Behairy[1†] M. El-Azab Farid[2‡] Awad A. Ibraheem[3,4§] Ola Ramadan[1] M. Anwar[1¶]

[1]Physics Department, Aswan University, Aswan 81528, Egypt
[2]Physics Department, Assiut University, Assiut 71516, Egypt
[3]Physics Department, King Khalid University, Abha, Saudi Arabia
[4]Physics Department, Al-Azhar University, Assiut 71524, Egypt

Abstract: In the context of the double folding optical model, the strong refractive effect for elastic scattering of ^{11}Li + ^{12}C and ^{11}Li + ^{28}Si systems at incident energies of 29, 50, and 60 MeV/n is studied. Real folded potentials are generated based on a variety of nucleon-nucleon interactions with the suggested density distributions for the halo structure of ^{11}Li nuclei. The rearrangement term (RT) of the extended realistic density dependent CDM3Y6 effective interaction is considered. The imaginary potential was taken in the traditional standard Woods-Saxon form. Satisfactory results for the calculated potentials are obtained, with a slight effect of the RT in CDM3Y6 potential. Successful reproduction with a normalization factor close to one for the observed angular distributions of the elastic scattering differential cross section has been achieved using the derived potentials. The obtained reaction cross-section is studied as a guide by extrapolating our calculations and previous results.

Keywords: optical model, elastic and inelastic scattering, halo nuclei, folding model, refraction effect

DOI: 10.1088/1674-1137/abca1b

I. INTRODUCTION

The study of halo nuclei that are far from the valley of β-stability and close to the nucleon drip-line has become one of the main topics in modern nuclear structure physics. This halo phenomenon for exotic nuclei has created much interest and hundreds of papers since its discovery in the mid-1980s. The halo of a nucleus arises from the very weak binding of the last one or two valence nucleons (protons or neutrons) to the core containing all other nucleons that are tightly bound; this weak binding energy leads to the creation of a neutron/proton tail. These halo nuclei have small separation energy as a result of the presence of a halo neutron/proton tail, extended nucleon density distributions, or quite large root mean square (rms) radii, and the emitted nucleons have narrow momentum distributions [1-3]. It has been proven that there are two types of halo nuclei: neutron and proton halos, which depend on the type of nucleon arrangements of the halo structure. Nuclei that have a one proton halo include ^{8}B and ^{26}P; those that have a one neutron halo are ^{11}Be and ^{19}C. Nuclei that have a two proton halo are exhibited by ^{17}Ne and ^{27}S [4-6], and those that have a two neutron halo include ^{6}He, ^{11}Li, ^{17}B, ^{19}B, and ^{22}C [7-11]. These halo nuclei consist of three body systems (an inert core nucleus plus two valence neutrons or two valence protons).

Exotic ^{11}Li nuclei have attracted much theoretical and experimental interest as a typical case. Their first production was described by Postanzer *et al.* in 1966 [12], and some special properties such as their large matter radii were discovered by Tanihata *et al.* [1, 13]. The ^{11}Li nucleus has numerous interesting properties. i) It consists of a core of three protons and six neutrons as well as a halo of two loosely bound neutrons; ^{11}Li belongs to the three-body system (^{9}Li+n+n), which is called a Borromean system [14, 15]. ii) The small separation energy (S_{2n}) of the two-neutron halo is only S_{2n}= 300 KeV [1], and in new research, it is found to be S_{2n}= 378±5 KeV [15, 16]. This small separation energy leads to an increase in the matter radius of ^{11}Li compared with other Li isotopes and forms a low-density halo, where nuclear radii increase with the mass number A of a nucleus as $A^{1/3}$. Further, it has been found that the matter radius of a ^{11}Li nucleus significantly deviates from the $A^{1/3}$ law, whereas other Li isotopes follow this law exactly [16]. iii) The rms radius is quite large compared to that of ^{9}Li (2.32±0.02) fm [13], which was found to be (3.12±0.16) fm [1, 13], and the latest measurements propose that it might be as large as (3.55±0.10) fm [2], where the size of the ^{11}Li nucleus is approximately equal to the size of ^{41}Ca and as large as

Received 3 August 2020; Accepted 14 October 2020; Published online 2 December 2020
† E-mail: Kass_phys@aswu.edu.eg
‡ E-mail: el_azab@aun.eun.eg
§ E-mail: awad_ah_eb@hotmail.com
¶ E-mail: melfawy99@aswu.edu.eg

^{208}Pb [16, 17], This means that two halo neutrons are mostly placed far from the ^{9}Li core. iv) It cannot be used as a target because it has a very short half-life time of 8.2 ms [18] for β^- decay. All these properties make the ^{11}Li nucleus an interesting halo nucleus that can be used as a projectile on several targets for studying the structure.

In the last several decades, numerous studies have generated widespread interest in the interaction cross section of the ^{11}Li nucleus as a projectile with several different targets [19-27]. The quasi-elastic scattering of ^{11}Li on ^{12}C was measured by Kolata *et al*. [20] at 60 MeV/n, and on ^{28}Si at 29 MeV/n by Lewitowicz *et al*. [21]. They used the coupled-channels (CC) method to reproduce the data, where the energy resolution did not allow for the separation of the true elastic scattering from inelastic scattering. A recent experiment for ^{11}Li scattering on ^{12}C was performed by Peterson *et al.* [22] at 50 MeV/n. They successfully separated the elastic and inelastic reaction channels in the critical forward-angle region. All the previous experimental studies [20-22] of quasielastic scattering of the neutron-halo nucleus of ^{11}Li with low-Z targets have reported and confirmed the strong refractive effect of this scattering process as first predicted by Satchler *et al.* [23]. This refractive effect has very long-range absorption due to ^{11}Li breakup, which increases the reaction cross section and is required for reproducing the experimental data. Mermaz [24] showed that it is necessary to use a surface potential that peaked very far outside the nucleus in order to reproduce the forward interference minimum core. The necessity of adding this long tail, which was introduced by Mermaz to the real part of the optical model potential to fit ^{11}Li scattering on ^{12}C and ^{28}Si, has been verified via *S*-matrix inversion techniques by Cooper and Mackintosh [25]. Several studies [19, 26, 27] treated the refractive long tail using the dynamic polarization potential (DPP) generated by the strong coupling of the breakup channels with the elastic one for ^{11}Li scattering. Khalili [27] proposed a theoretical interpretation of the data using Faddeev three-body wave functions within a four-body Glauber model; however, the results were not sensitive to details of the ^{11}Li wave function. The problem was that the required tail was much greater than that predicted by simple double folding (DF) model calculations, and the DPP corresponding to these models is repulsive in nature, rather than attractive.

Recently, the São Paulo potential (SPP) [28-31] has been used to successfully describe the elastic scattering and peripheral reaction channels for a large number of heavy-ion systems in a very wide energy region, as well as to describe the total reaction. In addition, it has been used for analyzing the elastic scattering of stable, weakly bound, and exotic nuclei on a variety of targets [32]. Khoa *et al.* [33] have generated the rearrangement term (RT) of the nucleon optical potential (OP) to modify the density and energy dependence of the CDM3Yn interactions, which succeeded in reproducing the Airy oscillation.

In this respect, we reanalyze the elastic scattering of ^{11}Li within a two-body model (core+halo) on ^{28}Si at 29 MeV/n and on ^{12}C at 50 and 60 MeV/n in an attempt to obtain an interpretation for the strong refractive effect within the ^{11}Li projectile structure. Our model is based on a semimicroscopic approach. The real part is calculated microscopically by folding several versions of M3Y effective nucleon-nucleon (*NN)* interaction (DDM3Y and CDM3Y6) in addition to the SPP. Three different densities for the ^{11}Li nucleus in conjunction with one density for ^{12}C and ^{28}Si targets are used. The imaginary part is calculated in the phenomenological Wood-Saxon (WS) form. Moreover, the effect of the RT in cross section calculations is investigated. The present paper is organized as follows. A theoretical formalism is presented in Sec. II, while Sec. III shows the results of analysis and discussion. Finally, concluding remarks are summarized in Sec. IV.

II. THEORETICAL FORMALISM

The optical nucleus-nucleus potential used in the present work is given by

$$U(R) = U_{\rm C}(R) + N_R V_{\rm DF}(R) + {\rm i}W_v(R), \tag{1}$$

where $U_{\rm C}(R)$ is the Coulomb potential, $V_{\rm DF}(R)$ is the DF real potential, and $W_v(R)$ is the imaginary potential in WS form. The real DF potential is calculated as

$$V_{\rm DF}(R) = \iint \rho_P\left(\vec{r_1}\right)\rho_T\left(\vec{r_2}\right)v_{NN}(S)\,{\rm d}\vec{r_1}{\rm d}\vec{r_2}, \tag{2}$$

where $\rho_P(r_1)$, $\rho_T(r_2)$ are the nuclear matter (NM) densities of the projectile and the target, respectively, while $v_{NN}(S)$ is the effective *NN* interaction between two nucleons, $S = \vec{R} - \vec{r_1} + \vec{r_2}$.

$$U_{\rm C}(R) = \frac{Z_1 Z_2 e^2}{2R_{\rm C}}\left(3 - \frac{R^2}{R_{\rm C}}\right) \quad \text{for} \quad R \leqslant R_{\rm C},$$
$$\text{or} \quad \frac{Z_1 Z_2 e^2}{R_{\rm C}} \quad \text{for} \quad R \geqslant R_{\rm C} \tag{3}$$

and the phenomenological imaginary WS potential is defined as

$$W(R) = \frac{W_0}{1 + \exp\left[\dfrac{R - R_i}{a_i}\right]}, \tag{4}$$

where W_0, R_i, and a_i are the depth, radius, and diffuse-

ness of the potential, respectively; $R_i = r_i\left(A_P^{\frac{1}{3}} + A_T^{\frac{1}{3}}\right)$, where i refers to V, W; and A_P and A_T are the projectile and target mass numbers, respectively.

A. Nuclear matter density distributions

For the projectile nucleus, three different density distributions are used, all of which consider that the structure of the ^{11}Li nucleus consists of ^{9}Li as the core and two halo neutrons. The first one is the cluster-orbital shell model approximation (COSMA), which can be expressed as [34]

$$\rho(r) = N_{CX}\frac{\exp\left(-r^2/a^2\right)}{\pi^{\frac{3}{2}}a^3} + N_{VX}\frac{2\exp\left(-r^2/a^2\right)}{3\pi^{\frac{3}{2}}b^5} \times\left[Ar^2 + \frac{B}{b^2}\left(r^2 - \frac{3}{2}b^2\right)^2\right],\ X = Z,N \tag{5}$$

where Z and N refer to the atomic number (protons) and number of neutrons, respectively, and N_{CX} and N_{VX} are fixed numbers, where N_{CX} refers to the number of protons and neutrons in the core nucleus, while N_{VX} refers to the number of neutrons in the halo term; A= 0.81, B = 0.19, N_{CZ}= 3, N_{CN} = 6, N_{VZ}= 0, N_{VN}= 2, a = 1.89 fm, and b = 3.68 fm [34].

The second density distribution is taken in the semi-phenomenological density (SPD) form, where the total matter density distribution can be taken as

$$\rho(r) = \rho_n(r) + \rho_p(r) \tag{6}$$

and

$$\rho_n(r) = \rho_{\rm core}(r) + \rho_{\rm tail}(r). \tag{7}$$

Since $\rho_{\rm core}(r)$ is the density of the neutrons in the core nucleus, while $\rho_{\rm tail}(r)$ represents the $2n$-halo neutron density distribution, the core part of both neutron and proton density distributions can be written as follows [35, 36],

$$\rho_i(r) = \frac{\rho_i^0}{1 + \left[\left(\frac{1+\left(\frac{r}{R}\right)^2}{2}\right)\right]^{\alpha_i}\left[\exp\left(\frac{(r-R)}{a_i}\right) + \exp\left(\frac{-(r+R)}{a_i}\right)\right]},\quad i = p,n \tag{8}$$

where p stands for protons, and n for neutrons. The central densities ρ_p^0 and ρ_n^0 are determined from the normalization conditions:

$$4\pi\int\rho_n(r)r^2{\rm d}r = N, \tag{9}$$

$$4\pi\int\rho_p(r)r^2{\rm d}r = Z, \tag{10}$$

where N (Z) is the total number of neutrons (protons) in the nucleus, and the other parameters (α_i, a_i) can be determined in detail using Refs. [35, 36]. The tail/halo part can be written as [35]

$$\rho_{\rm tail}(r) = N_0\left(\frac{r^2}{(r^2+R^2)^2}\right)\exp\left(\frac{-r}{a_t}\right), \tag{11}$$

where N_0 is determined from the normalization

$$4\pi\int\rho_{\rm tail}(r)r^2{\rm d}r = 2, \tag{12}$$

where 2 refers to the number of halo neutrons. Finally, the third density distribution form is that deduced using the simpler non-relativistic Hartree-Fock (HF) model [37].

For ^{12}C and ^{28}Si target nuclei, only the two-parameter Fermi model (FM) is used [38]

$$\rho_T^{^{12}{\rm C}(^{28}{\rm Si})} = \frac{0.207\,(0.175)}{1+\exp\left[\left(\frac{r-2.1545\,(3.15)}{0.425\,(0.475)}\right)\right]}, \tag{13}$$

where the rms radii, which are extracted from this density, are 2.298 and 3.012 fm for ^{12}C and ^{28}Si, respectively.

B. *NN* effective interactions

Based on the M3Y interaction, which is designed to reproduce the G-matrix elements for Paris and Reid [39, 40] effective NN interactions, two versions of the M3Y effective NN interaction are used. These versions depend on two different forms of the density and energy-dependence (DDM3Y and CDM3Y6). In addition to the SPP, the CDM3Y6 interaction, which was recently modified by the RT [33], is also used. The first method is the DDM3Y effective interaction, defined as [38]

$$\upsilon(E,\rho,S) = g(E,S)F(E,\rho), \tag{14}$$

where

$$F(E,\rho) = C(E)[1+\alpha(E)\exp(-\beta(E)\rho)], \tag{15}$$

C, α, and β are the energy dependent parameters, and$\rho = (\rho_P + \rho_T)$. The factor $g(E,S)$ is represents the original zero range M3Y-Reid NN interaction [38], which

can be written in the form

$$g(E,S)=\upsilon_D(R)+\hat{J}(E)\delta(S), \tag{16}$$

where E is the laboratory energy per projectile nucleon, $\vec{s}$ is the inter-nucleon separation, $\delta(s)$ is the delta function, $\hat{J}(E)$ represents the effects of the knock-on exchange between interacting nucleons, and $\upsilon_D(r)$ represents the direct parts. The term $\hat{J}(E)$ is taken as [38]

$$\hat{J}(E)=-276\left[1-0.005\left(E/A\right)\right]\ \text{MeV.fm}^3, \tag{17}$$

with the direct part in the M3Y-Paris as

$$\upsilon_D(R)=\left[11062\frac{\exp(-4R)}{4R}-2538\frac{\exp(-2.5R)}{2.5R}\right]\ \text{MeV}. \tag{18}$$

The next *NN* effective interaction used is the other density dependent version (CDM3Y6) for the direct and exchange terms, where the full CDM3Y6 interaction form is defined as [41]

$$\upsilon_{D(Ex)}(\rho,R)=g(E)F(\rho)\upsilon_{D(Ex)}(R), \tag{19}$$

where the direct part $\upsilon_D(r)$ is that in Eq. (18), and the knock-on exchange parts in the infinite-range exchange are taken as

$$\upsilon_{Ex}(R)=\left[-1524\frac{\exp(-4R)}{4R}-518.8\frac{\exp(-2.5R)}{2.5R}-7.847\frac{\exp(-0.7072R)}{0.7072R}\right]\ \text{MeV}, \tag{20}$$

with the function $F(\rho)$ written as [41, 42],

$$F(\rho)=0.2658\left[1+3.8033\exp(-1.41\rho)-4.0\rho\right], \tag{21}$$

and $g(E)$ is the energy dependent factor, given by [41]

$$g(E)=\left[1-0.003\left(E/A\right)\right]. \tag{22}$$

For reproducing the saturation properties of symmetric NM in the standard HF calculation, and to have a reliable density dependent interaction for use at different energies (the high-momentum part of the HF single-nucleon potential), the modified CDM3Y6 interaction (CDM3Y6-RT) with the RT contribution has been carried out. The density dependence of $\Delta F(\rho)$ obtained from the exact expression of the RT given as [33]

$$\Delta F(\rho)=1.5\left[\exp(-0.833\rho)-1\right]. \tag{23}$$

In contrast, we use the SPP, where the radial and energy dependence is written as follows [43]:

$$V(R,E)=V_F(R)\exp\left(-4\beta^2\right), \tag{24}$$

where $\beta=v/c$, v is the local relative velocity between the two nuclei, and $V_F(R)$ is a folding potential, such as the expression in Eq. (2) where $\upsilon_{nn}(S=\vec{R}-\vec{r_1}-\vec{r_2})$ is a physical *NN* interaction given by $\upsilon_{nn}(S)=V_0\delta(S)$ using $V_0=-456$ MeV fm^3, and the usage of the delta function corresponds to the zero range approach. Systemizations of the nuclear densities were achieved in Ref. [44], providing a good explanation of matter and charge distribution. In this work, for the target ^{12}C, we assume that $a_m=0.53$ fm and $a_c=0.56$ fm for the matter and charge diffuseness, respectively. The matter and charge distribution radii are given by $R_M=1.3A^{1/3}-0.84$ and $R_C=1.76Z^{1/3}-0.96$, respectively. The matter density of the projectile nucleus is used as tabulated in numerical form.

III. PROCEDURE

The analysis of ^{11}Li+^{12}C, ^{28}Si elastic scattering is carried out by using the OPs generated from Eq. (1). The DF real parts of the OPs are evaluated using several versions of the M3Y density- and energy dependent effective interactions such as DDM3Y (14), CDM3Y6 (19), and CDM3Yn-RT (23), in addition to the SPP. The imaginary potential is calculated using Eq. (4) as a phenomenological WS form with three parameters. The obtained potentials are then fed into the HIOPTM-94 [45] computer code to calculate the elastic scattering differential cross sections. For obtaining the best fit, searches on the potential parameters are performed using the HIOPTM-94 code to achieve the minimum χ^2 value, defined as [46, 47]

$$\chi^2=\frac{1}{N}\sum_{K=1}^{N}\left[\frac{\sigma_{\text{th}}(\theta_K)-\sigma_{\text{ex}}(\theta_K)}{\Delta\sigma_{\text{ex}}(\theta_k)}\right]^2, \tag{25}$$

$\sigma_{\text{th}}(\sigma_{\text{ex}})$ is the theoretical (experimental) cross section at an angle θ_K in the c.m. system, $\Delta\sigma_{\text{ex}}$ is the experimental error, and N is the number of the data points. For the experimental errors of all measured data, an average value of 10% is used. For semi-microscopic analysis, searches are carried out on four parameters (the real renormalization factor (N_R) in conjunction with the three WS imaginary potential parameters W_0, R_i and a_i). In contrast, for the phenomenological WS approach, searches are performed on six free parameters (three WS real potential parameters, V_v, R_v, and a_v, and three imaginary potential parts, W_0, R_i, and a_i).

IV. RESULTS AND DISCUSSION

A. Potentials and densities

The radial shapes of the considered different types of density distributions of ^{11}Li are shown in Fig. 1, in linear and logarithmic scale. The corresponding calculated rms radii of protons, neutrons, and matter for all used density distributions of the ^{11}Li nucleus are listed in Table 1, as compared with previous works and experimental data. The present results agree with the previous calculations that predict a long tail halo for the ^{11}Li nucleus, in comparison with the experimental data, as summarized in Table 1. Further, our calculations agree well with the previous rms values; however, there is a slight difference compared with the experimental data. Moreover, previous studies have extracted these quantities [24, 48-51], which agree with the present calculations, but it is noticed that, in the important study of Mermaz [24], the value $\langle R_m \rangle^{\frac{1}{2}} = 3.74$ was extracted, which is greater than the experimental and other theoretical calculations.

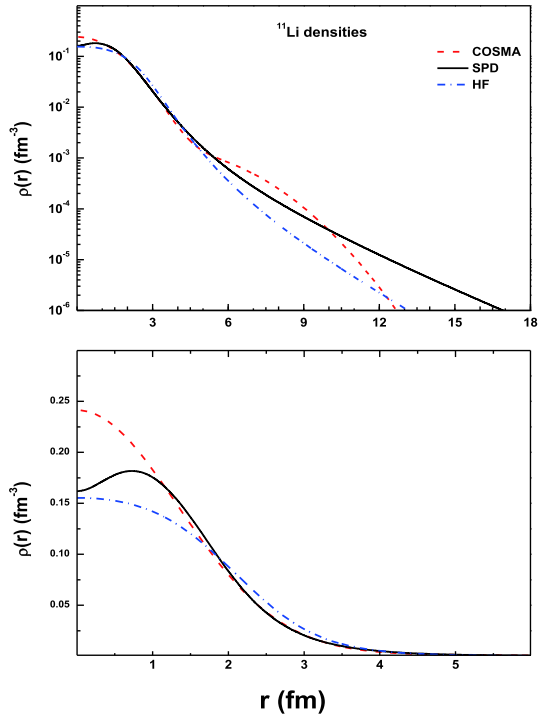

Fig. 1. (color online) The densities of ^{11}Li with logarithmic and linear scales.

The results of the considered density distributions are illustrated in Fig. 1. It can be seen that COSMA density has a larger value than those of the SPD and HF at small distances ($r \leqslant 1$ fm), while the latter density has the smallest value. At large distances ($r \geqslant 10$ fm), we can see that all the used densities have a long tail due to the structure of ^{11}Li as a core with two valence neutrons. The SPD density has the longest tail, so it gives a successful description for the largest radius of ^{11}Li. In contrast, investigation of the halo densities for the ^{11}Li nucleus and the considered *NN* effective interaction effects is performed through the calculation of the DF potential of Eq. (2). The real parts of the OPs are calculated with the DDM3Y, CDM3Y6, and CDM3Y6-RT effective NN interactions in addition to the SPP folded with the considered three densities, COSMA, SPD, and HF, at energies of 50 and 60 MeV/n, for ^{11}Li scattered by ^{12}C, and at 29 MeV/n, for the ^{11}Li+ ^{28}Si system. The physical observations related to the resulted potentials for ^{12}C at an energy of 60 MeV/n are presented in Table 2 and Fig. 2, as one case.

The folded potentials in the present work are calculated as a sum of two parts for projectile (^{11}Li) density, and halo (neutrons) density plus core density is folded with target density and *NN* effective interaction. The effects of different densities of ^{11}Li structure and the considered effective interaction on our potential model represent our focused study point.

Generally, as we have seen from Fig. 2 and Table 2, the folded potentials using the considered densities and effective interaction have approximately the same depths and behavior for the density-dependent effective *NN* interaction with a slight difference. From Table 2, we notice that the long potential rms is to be achieved with COSMA and SPD densities, CDM3Y6-RT, and DDM3Y effective interactions, while the smallest potential tail is to be achieved with HF density, SPP, and CDM3Y6 effective interactions. In addition, the energy dependence for the real potential volume integral of the ^{12}C target is observed, where it decreases with increasing energy. Fig. 2 confirms these results, where the SPP gives the largest depth compared to those using the DDM3Y and

Table 1. Calculated rms proton (R_p), neutron (R_n), and mass ($R_{\rm rms}$) radii in fermis for the three NM densities of the ^{11}Li nucleus.

density	R_p		R_n		$R_{\rm rms}$	
	calc.	Ref.	calc.	Ref.	calc.	Ref.
COSMA	2.32	2.32 [35]	3.62		3.318	3.21 [51]
SPD	2.16	2.17 [36]	3.67	3.67 [36] 3.21 [13]	3.325	3.32 [36] 3.12 [1, 13]
HF	2.24		3.08		2.872	2.846 [48]
exp.	2.88±0.11 [13]		3.21±0.17 [13]		3.12±0.16 [13]	

Table 2. The calculated volume integrals and rms radii of the folded potentials for ^{11}Li+^{12}C, ^{28}Si systems at 50 and 60 MeV/n for ^{12}C and 29 MeV/n for ^{28}Si, using the four *NN* effective interactions with the three densities without N_R.

E/(MeV/n)	density	-J/(MeV fm^3)				R_{rms}/fm			
		CDM3Y6	CDM3Y6-RT	SPP	DDM3Y	CDM3Y6	CDM3Y6-RT	SPP	DDM3Y
				^{11}Li + ^{12}C					
	COSMA	301.12	271.42	271.0	252.74	4.692	4.88	4.40	4.789
50	SPD	300.84	271.28	275.5	251.99	4.691	4.86	4.45	4.772
	HF	302.57	274.86	271.4	254.37	4.272	4.41	4.03	4.358
	COSMA	281.71	256.50	254.5	235.63	4.694	4.89	4.39	4.799
60	SPD	281.50	262.70	257.1	234.99	4.693	4.87	4.33	4.772
	HF	283.31	259.91	253.2	237.43	4.278	4.42	3.90	4.360
				^{11}Li + ^{28}Si					
	COSMA	358.79	311.71	314.7	297.64	5.128	5.31	4.79	5.20
29	SPD	358.07	311.30	309.4	296.43	5.127	5.29	4.65	5.18
	HF	359.04	314.73	314.1	297.49	4.737	4.87	4.45	4.81

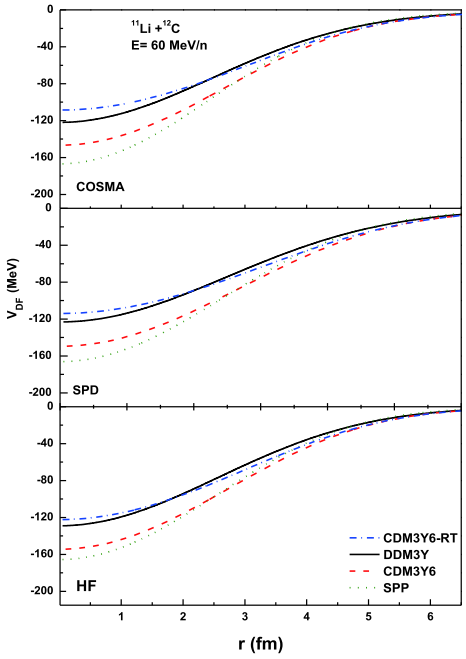

Fig. 2. (color online) The real DF for ^{11}Li+^{12}C at 60 MeV/n using the three densities with DDM3Y, CDM3Y6, and CDM3Y6-RT effective NN interactions and the SPP with N_R=1.0 with a linear scale.

CDM3Y6, while CDM3Y6-RT gives the smallest value among all; this arises in the interior region at r (r < 2 fm). The folded potentials of the other (50 MeV/n) energies and those for the ^{28}Si target at 29 MeV/n have the same behavior as those at 60 MeV/n, but with different depths, where the depths of the potentials increase with decreasing energy. The obtained potential agrees well with the systematic suggested potential models based on the break up potential of Yabana [52], the DP potential of Khalili [27], and the folded potentials of Khoa [26]. However, the extracted real folded potentials have a shorter tail in facing the successful Mermaz potential [24].

B. Differential cross sections

Many attempts have been made to generate appropriate OPs for analyzing the angular distribution cross section of ^{11}Li projectile reactions. The result drawn from all previous theoretical studies [19, 23-27] is that the nearside/farside interference minimum is missing or greatly attenuated in the elastic scattering of ^{11}Li with low-Z targets at intermediate energies. The presence of a sharp minimum at 4^0 in the calculated angular distributions was due to the contamination by ^{9}Li ions resulting from projectile breakup [22]. The successful theoretical work that explained this discrepancy at forward angles was proposed by Mermaz [24] using phenomenological potential with coupling for low excited inelastic channels and many adjusted free parameters.

The same type of analysis as previously used has been presented, that is, the one with WS potential. To improve the agreement with the considered experimental data, we employ the widely used phenomenological WS potential with six parameters. More parameters in such a famous model means more flexibility in order to obtain the best fit that can be used later as a guide. The elastic scattering for the ^{11}Li nucleus from ^{12}C at the two energies, 50 and 60 MeV/n, and that from ^{28}Si at 29 MeV/n have been analyzed in the framework of the conventional optical model by using the standard WS form, as in Eq. (4). Moreover, a semi-microscopic optical DF folding potential has been generated to study the sensitivity of *NN* interaction, as well as the form of the halo density distributions of ^{11}Li on reaction differential cross sections. The obtained results are listed in Tables 3 to 5 and shown in Figs. 3 to 6.

The results of angular distributions obtained using the WS optical model are compared with experimental data in Fig. 3, and their potential parameters are listed in Table 3. As shown in Fig. 3(a), the best fit with experimental data has been achieved for the ^{28}Si target without an anomaly at near or far angles. The results are more successful than those of previous studies that used a combination of elastic and inelastic parts to achieve a reasonable result [21]. In contrast, a reasonable fit with data has been obtained for the ^{12}C target at the two energies, 50 and 60 MeV/n, as shown in Fig. 3(b, c), but with a sharp minimum between (2.5)° and 4°.

The results displayed in Tables 4 and 5 as well as Figs. 4 to 6 have been obtained using the semi-micro-

Table 3. Best fit OP parameters of the WS model.

E/(MeV/n)	V/MeV	r_v/fm	a_v/fm	W/MeV	r_i/fm	a_i/fm	-J/(MeV fm^3)		χ^2	σ_R
							J_R	J_I		
^{11}Li + ^{12}C										
50	116.4	0.83	0.81	2.83	2.19	0.057	286.03	86.68	13.0	2009
60	295.92	0.21	1.35	20.72	0.92	1.20	233.33	86.12	5.2	1400
^{11}Li + ^{28}Si										
29.0	261.91	0.41	1.78	7.029	2.29	0.362	201.57	33.05	2.96	1495

Table 4. The best fit parameters obtained for elastic scattering data for the ^{11}Li+^{12}C system at energies of 50 and 60 MeV/n using NN interaction (DDM3Y, CDM3Y6, CDM3Y6-RT, and SPP) with the considered three densities (COSMA, SPD, and HF).

E/(MeV/n)	density	potential	N_R	-J/(MeV fm^3)		W/MeV	r_i/fm	a_i/fm	χ^2	σ_R
				J_R	J_I					
50	COSMA	CDM3Y6-RT	1.18	320.27	104.23	4.529	1.889	1.122	11.17	2300
		DDM3Y	1.15	289.27	105.71	4.926	1.840	1.124	14.60	2273
		CDM3Y6	0.92	278.36	95.06	4.393	1.852	1.092	12.96	2146
		SPP	0.86	233.51	80.11	4.727	1.675	1.169	14.72	1872
	SPD	CDM3Y6-RT	1.16	314.55	105.07	4.217	1.959	1.041	13.97	2324
		DDM3Y	1.13	283.91	110.30	4.724	1.905	1.086	17.36	2356
		CDM3Y6	0.91	274.07	99.950	4.219	1.925	1.031	15.68	2229
		SPP	0.93	257.02	100.27	4.818	1.799	1.225	16.45	2236
	HF	CDM3Y6-RT	1.06	291.83	103.05	3.900	2.019	0.918	14.57	2290
		DDM3Y	1.06	270.07	111.37	4.382	1.977	1.012	17.85	2389
		CDM3Y6	0.87	261.79	101.15	3.946	1.994	0.946	16.20	2258
		SPP	0.85	229.75	94.16	4.150	1.867	1.188	18.21	2190
60	COSMA	CDM3Y6-RT	1.18	303.45	136.83	50.00	0.674	1.371	6.21	1737
		DDM3Y	1.20	283.39	124.32	49.57	0.650	1.342	6.03	1625
		CDM3Y6	0.94	264.15	116.92	44.16	0.725	1.214	5.82	1484
		SPP	0.85	215.98	92.40	39.03	0.750	1.032	6.61	1187
	SPD	CDM3Y6-RT	1.12	293.94	140.90	60.06	0.569	1.459	7.19	1811
		DDM3Y	1.18	276.33	126.92	53.02	0.607	1.400	6.76	1678
		CDM3Y6	0.92	258.60	120.01	47.52	0.684	1.269	6.50	1536
		SPP	0.85	213.14	95.12	39.81	0.742	1.066	6.74	1228
	HF	CDM3Y6-RT	1.05	272.94	137.63	50.00	0.676	1.373	7.73	1741
		DDM3Y	1.07	254.89	131.36	84.24	0.384	1.490	7.33	1720
		CDM3Y6	0.84	238.26	124.09	67.91	0.517	1.355	7.11	1572
		SPP	0.80	204.70	101.33	50.90	0.628	1.182	7.24	1313

Table 5. The best fit parameters for the elastic scattering data for the ^{11}Li+^{28}Si system at an energy of 29 MeV/n using *NN* interaction (DDM3Y, CDM3Y6, CDM3Y6-RT, and SPP) with the considered three densities (COSMA, SPD, and HF).

E/(MeV/n)	density	potential	N_R	-J/(MeV fm^3)		W/MeV	r_i/fm	a_i/fm	χ^2	σ_R
				J_R	J_I					
29	COSMA	CDM3Y6-RT	0.64	198.76	45.12	14.69	2.188	0.767	4.53	1460
		DDM3Y	0.82	242.49	52.12	15.65	2.235	0.709	4.53	1528
		CDM3Y6	0.69	247.20	50.45	15.40	2.227	0.728	4.60	1518
		SPP	0.899	282.99	46.04	14.79	2.198	0.772	5.00	1485
	SPD	CDM3Y6-RT	0.62	193.58	45.23	15.73	2.174	0.795	5.31	1457
		DDM3Y	0.81	238.51	51.81	15.61	2.234	0.718	5.01	1527
		CDM3Y6	0.68	243.41	50.53	15.60	2.220	0.740	5.34	1516
		SPP	0.896	277.11	46.15	14.82	2.198	0.770	5.85	1483
	HF	CDM3Y6-RT	0.58	181.83	45.95	16.60	2.128	0.849	6.37	1442
		DDM3Y	0.77	229.06	52.00	16.11	2.218	0.736	5.62	1517
		CDM3Y6	0.64	233.83	50.95	16.16	2.204	0.750	6.22	1504
		SPP	0.87	273.86	51.08	17.76	2.148	0.803	7.17	1481

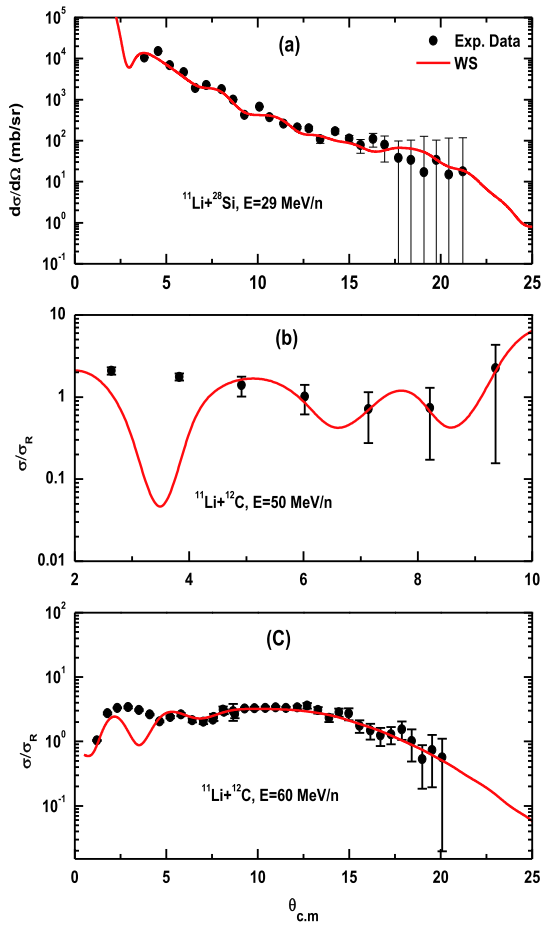

Fig. 3. (color online) The best fit angular distribution of ^{11}Li scattered elastically from ^{12}C and ^{28}Si calculated with the WS potential model. The symbol represents the experimental data taken from Refs. [20-22].

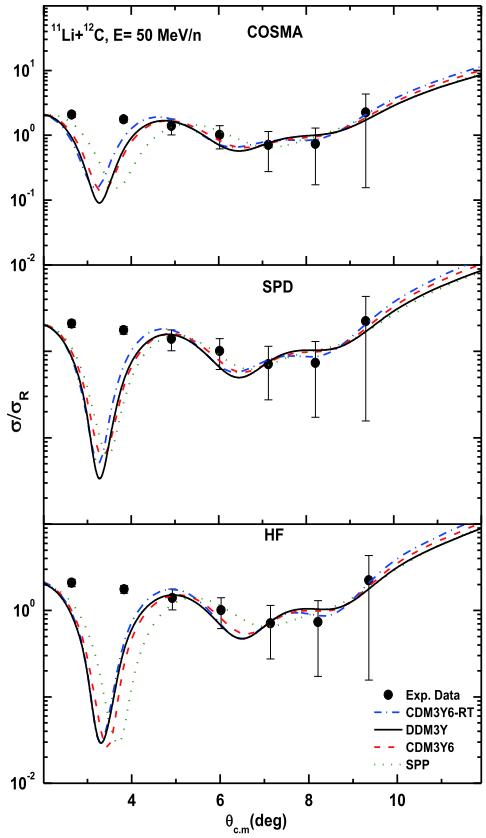

Fig. 4. (color online) The best fit angular distributions of elastic scattering of ^{11}Li from ^{12}C at 50 MeV/n calculated with the semi-microscopic real DF potentials, CDM3Y6-RT (dashed-dotted line), DDM3Y (sold line), CDM3Y6 (dashed line), and SPP (dotted line). The symbol is a representation of the experimental data from Ref. [22]. Upper panel for COSMA density, middle panel for SPD density, and bottom panel for HF density.

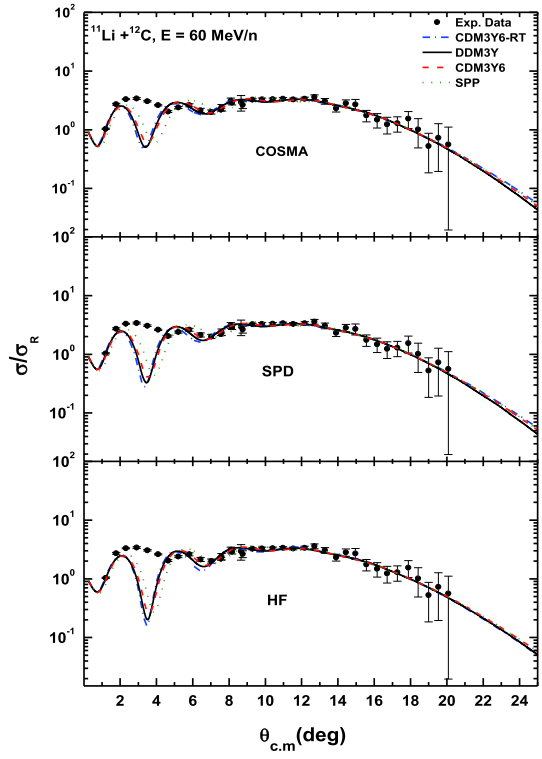

Fig. 5. (color online) Same as Fig. 4, but for energy 60 MeV/n. The experimental data are taken from Ref. [20].

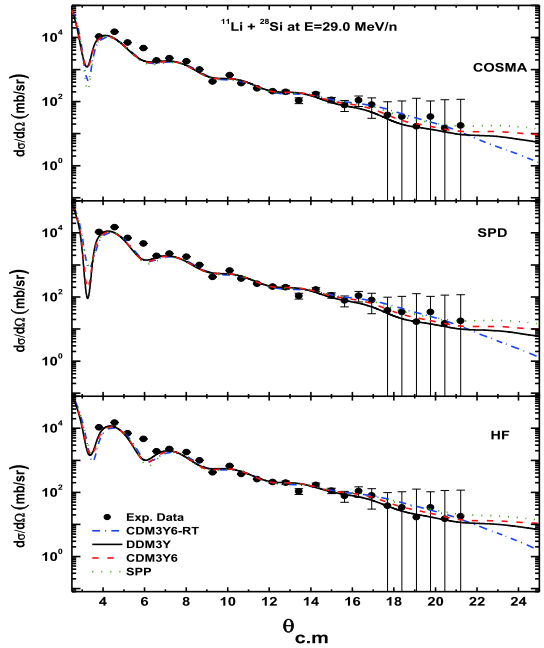

Fig. 6. (color online) Same as Fig. 4, but for the elastic scattering of ^{11}Li from ^{28}Si at energy 29 MeV/n. The experimental data are taken from Ref. [21].

scopic potentials. Firstly, it is noticed that the N_R coefficients are close to one, i.e., 1.0±0.01 for energies 50 and 60 MeV/n for the ^{12}C target and 0.8±0.01 for the ^{28}Si target, providing a satisfactory agreement with experimental data. These results are more successful than those achieved in previous studies that used the CC model [21], quasielastic potential [26], Glauber of four body model [27], the breakup effect [51], and the JLM potential [53].

Generally, the results corresponding to Figs. 4 to 6 show that the considered effective interactions and densities predict the best agreement with the experimental results. It is clear that the three angular distributions resulting from DDM3Y, DDM3Y6, and DDM3Y6-RT are very similar to each other; however, a small shift in the forward angle between $(2.5)^0$ and 4^0 for SPP is noticed.

Figure 4 shows the results in comparison with the measured experimental data for the ^{12}C target at an energy of 50 MeV/n, where the agreement with the data is reasonable and is of higher quality than that obtained from the quasielastic calculation of Peterson *et al.* [22]. Likewise, Fig. 5 shows the good agreement of the predictions of our calculations with the experimental data for the ^{12}C target at an energy of 60 MeV/n, in comparison with those from previous attempts by many authors [26, 27, 52, 53]. Meanwhile, the same results for the ^{28}Si target at an energy of 29 MeV/n, which agree more with the experimental data than the results of [21, 48, 53, 54], have been obtained, as shown in Fig. 6. Despite the success achieved in the data analysis for practical data, anomalies at small angles still exist. In this angular range, the optical model amplitude is insensitive to the potential used due to a breakdown of the optical model in the explanation of the small-angle cross section for the halo nucleus, which could be attributed to the extreme peripheral nature of these reactions at intermediate energies due to the surface transparent potential.

C. Total reaction cross sections

In order to understand the formation of a halo around the core of radioactive nuclei, which is very difficult, it is useful to study the reaction cross section (RCS) in addition to differential cross sections of the exotic nucleus ^{11}Li from targets. The RCS σ_R represents an important constraint on the OP calculation. The average total RCSs σ_R for the present calculations are listed in Table 6. The behavior of the reaction mechanism is extrapolated for a range of low and high energies (30, 75 and 85 MeV/n). These results are listed together with the previous values [19, 21, 23, 26, 48, 52], in conjunction with the experimental values of Refs. [55-57], and are illustrated in Fig. 7. Unfortunately, σ_R was not measured at 50 MeV/n.

As seen in Table 6, the present calculated σ_R generally agrees with the previous theoretical calculations, and on average, our results in Fig. 7 are closer to the experimental cross sections measured or those estimated from the systematics at relevant bombarding energies for the ^{12}C target. The calculated energy dependence of the total cross sections is well approximated by the expression

Table 6. The calculated mean value and the previous calculations comparable to the experimental results of the reaction cross section σ_R (mb) for ^{11}Li+^{12}C, ^{28}Si systems at 50 and 60 MeV/n for ^{12}C and 29 MeV/n for ^{28}Si.

target	*E*/*A*	present cal.	previous	
			cal.	exp.
^{12}C	30	2942 ±2	1710 [23]	2947 [55]
	50	2238.58±10.68	–	–
	60	1552.67±16.79	1274±30 [26] 1391±35 [19] 1520 [52]	1500±50 [56, 57]
	75	1449±3	1401 [26]	1430±60 [56]
	87.0	1264 ±2	1264 [26]	1260±40 [57]
^{28}Si	29	1493.17±2.45	1402 [21] 1970 [48] 1520 [52]	2947±386[a] [48]

[a] Measured at 25.5 MeV/n.

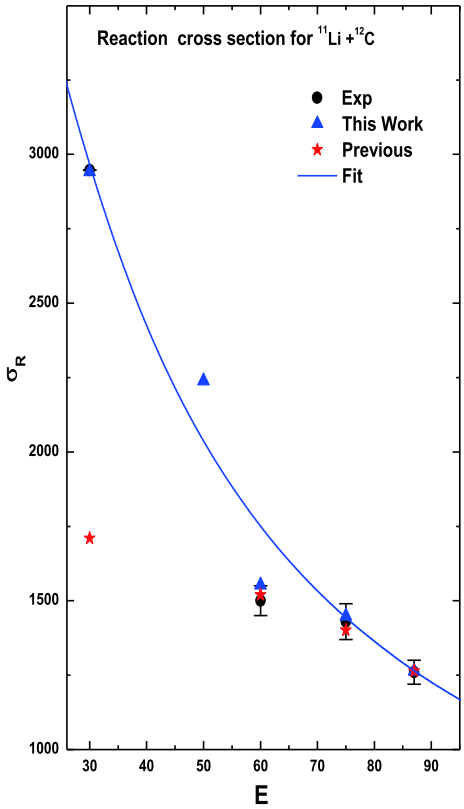

Fig. 7. (color online) Energy dependence of the reaction cross section in the optical limit of the DF model using the present model for ^{11}L+^{12}C. The triangles denote the mean obtained results with considered potentials, the star shapes denote the previous calculations, and the circles denote the experimental data taken from Refs. [48, 55-57].

$$\sigma_R^{\text{cal.}}(E) = 1.3\pi\left(A_p^{\frac{1}{3}} + A_T^{\frac{1}{3}}\right)^2\left(\frac{1459.4}{E} - \frac{11621.4}{E^2}\right), \qquad (26)$$

where E represents the value of energy per nucleon. It is obvious from Fig. 7 and the results listed in Table 6 that the behavior of the generated results reflects the success of our potentials in reproducing the exotic nuclei reactions. For the ^{28}Si target, while the present results of σ_R agree with previous theoretical calculations, they are lesser than the results of the experimental data. The reason for this discrepancy could be the effect of the coupling of the low-lying exited states of ^{28}Si to the elastic channels, which must be included or separated from the elastic events by those inelastic states. In addition, the value $\sigma_R = 2947 \pm 386$ mb corresponds to an energy of 25.5 MeV/n.

V. CONCLUSION

Explaining the discrepancy between the experimental and calculated differential cross sections at forward angles for the interaction of ^{11}Li with low-Z targets at intermediate energies can be divided into two stages. First, the studies could not predict this anomaly as a highly refractive nature for a quasi-elastic scattering process. Second, successful results were generated by Meermaz [24] and confirmed by the recent experimental study of Peterson *et. al.* [22], in which the elastic and inelastic reaction channels were cleanly separated in the forward angle. They verified that the ^{9}Li contamination data are responsible for the displayed interference minima. The purpose of the present paper is to provide a new attempt to describe the elastic scattering of ^{11}Li from ^{12}C and ^{28}Si through DF.

In the context of the DF optical model potential and as an extension of our studies [58-60], the elastic scattering of ^{11}Li+^{12}C and ^{11}Li+^{28}Si has been reanalyzed. The nucleus-nucleus interaction potential has been constructed microscopically from folding the density-dependent effective *NN* interactions DDM3Y, CDM3Y6, and SPP over the NM distributions of the interacting nuclei. The resulting potentials are used as the real part of the OP, while the imaginary component is treated phenomenolo-

gically through the WS form to calculate the angular distributions of the elastic scattering differential cross sections. Successful predictions were obtained by using our potentials generated for different energies within the measured angular ranges. The results indicate that using a unified energy dependent real potential is adequate to successfully fit the data in the considered energy range. Looking at the chi-square values mentioned in the above tables, we found that, with different versions for the NM density of the lithium nucleus, the smallest values at energies 50 and 60 MeV were obtained using CDM3Y6-RT and CDM3Y6, respectively.

Due to the repulsive contribution of the RT to the real folding potential, especially at a small internuclear distance, this contribution has been shown to be vital in the application of the folding model to the study of elastic ^{11}Li+^{12}C and ^{11}Li+^{28}Si scattering in order to obtain the realistic shape and strength of the real potentials. The prediction capability of the folding model for ^{11}Li+^{12}C and ^{11}Li+^{28}Si is good. For this type of foldingpotential, systematic folding model studies of the elastic and inelastic nucleus-nucleus scattering over a wide range of energies are encouraged.

In contrast, the total reaction cross sections for the considered reactions together with extended energies are investigated. It is observed that the RCS increases linearly with rising energy at lower energies. It is also noted that both the observed data and those theoretically obtained from previous elastic scattering studies are in good agreement with the values generated by the current elastic scattering calculations.

Finally, we can argue that the simple calculated semimicroscopic potential of the DF model is considered as an advanced result and is more accurate compared with those from the previous complicated studies. The present results encourage us to modify the present potential calculation approach for full microscopic analysis to explain the discrepancy of the interaction of ^{11}Li with low-Z targets at intermediate energies and to extend the analysis to other halo reactions.

References

[1] I. Tanihata, H. Hamagaki, O. Hashimoto *et al*., Phys. Rev. Lett. **55**, 2676 (1985)
[2] J. S. Al-Khalili and J. A. Tostevin, Phys. Rev. Lett. **76**, 3903 (1996)
[3] A. Jensen, K. Riisager, D.V. Fedorov *et al*., Rev. Mod. Phys. **76**, 215 (2004)
[4] Y. L. Parfenova and M.V. Zhukov, Phys. Rev. C **66**, 064607 (2002)
[5] M. V. Zhukov and I. J. Thompson, Phys. Rev. C **52**, 3505 (1995)
[6] E. Garrido, D. V. Fedorov, and A. S. Jensen, Nucl. Phys. A **733**, 85 (2004)
[7] A. Cobis, D. V. Fedorov, and A. S. Jensen, Phys. Rev. C **58**, 1403 (1998)
[8] F. M. Nunes, J. A. Christley, I. J. Thompson *et al*., Nucl. Phys. A **609**, 43 (1996)
[9] C. Remero-Redondo, E. Garrido, D. V. Fedorov *et al*., Phys. Rev. C **77**, 054313 (2008)
[10] T. Tarutina, I. J. Thompson, and J. A. Tostevin, Nucl. Phys. A **733**, 53 (2004)
[11] W. Horiuchi and Y. Suzuki, Phys. Rev. C **74**, 34311 (2006)
[12] A. M. Poskanzer, S. W. Cosper, E. K. Hyde *et al*., Phys. Rev. Lett. **17**, 1271 (1966)
[13] I. Tanihata, T. Kobayashi, O. Yamakawa *et al*., Phys. Lett. B **206**, 592 (1988)
[14] M. V. Zhukov, B. V. Danilin, D. V. Fedorov *et al*., Phys. Rep. **231**, 151 (1993)
[15] C. Bachelet, G. Audi, C. Gaulard *et al*., Phys. Rev. Lett. **100**, 182501 (2008)
[16] Hiroyuki Sagawa and Kouichi Hagino, Eur. Phys. J. A **51**, 102 (2015)
[17] B. Jonson, Phys. Rep. **389**, 1 (2004)
[18] R. Klapischr, C. Thibault-Philippce, C. Drtrazc *et al*., Phys. Rev. Lett. **23**, 652 (1969)
[19] I. J. Thompson, J. S. Al-Khalili, J. A. Tostevin *et al*., Phys. Rev. C **47**, R1364 (1993)
[20] J. J. Kolata, M. Zahar, R. Smith *et al*., Phys. Rev. Lett. **69**, 2631 (1992)
[21] M. Lewitowicz *et al*., Nucl. Phys. A **562**, 301 (1993)
[22] D. Peterson, J. J. Kolata, P. Santi *et al*., Phys. Rev. C **67**, 014601 (2003)
[23] G. R. Satchler, K. W. McVOY' and M. S. HUSSEIN, Ncul. Phys. A **522**, 621 (1991)
[24] Mechil C. Mermaz, Phys. Rev. C **47**, 2213 (1993)
[25] S. G. Cooper and R. S. Mackintosh, Nucl. Phys. A **582**, 283 (1995)
[26] Dao T. Khoa, G. R. Satchler and W. von Oertzen, Phys. Lett. B **358**, 14 (1995)
[27] J. S. Al-Khalili and J. A. Tostevin, Phys. Rev. C **49**, 386 (1994)
[28] L. C. Chamon, D. Pereira, M. S. Hussein *et al*., Phys. Rev. Lett. **79**, 5218 (1997)
[29] L. C. Chamon, D. Pereira, M. S. Hussein, Phys. Rev. C **58**, 576 (1998)
[30] M. A. G. Alvarez, L. C. Chamon, D. Pereira *et al*., Nucl. Phys. A **656**, 187 (1999)
[31] L. C. Chamon, Nucl. Phys. A **787**, 198c (2007)
[32] M. A.G. Alvarez, N. Alamanos, L.C. Chamon *et al*., Nucl. Phys. A **753**, 83 (2005)
[33] Dao T. Khoa Nguyen Hoang Phuc, Doan Thi Loan and Bui Minh Loc, Phys. Rev. C **94**, 034612 (2016)
[34] A. N. Antonov, M. K. Gaidarov, D. N. Kadrev *et al*., Int. J. Mod. Phys. E **13**, 759 (2004)
[35] A. Bhagwat, Y. K. Gambhir, and S. H. Patil, Eur. Phys. J. A **8**, 511 (2000)
[36] A. Bhagwat, Y. K. Gambhir, and S. H. Patil, J. Phys. G: Nucl. Part. Phys. **27**, B1 (2001)
[37] D. Vautherin and D. M. Brink, Phys. Rev. C **5**, 626 (1972)
[38] M. El-Azab Farid and G. R. Satchler, Nucl. Phys. A **438**, 525 (1985)
[39] G. F. Bertsch, J. Borysowicz, H. Mcmanus and W. G. Ae, Nucl. Phys. A **284**, 399 (1977)
[40] N. Anantaraman, H. Toki and G. F. Bertsch, Nucl. Phys. A **398**, 269 (1983)
[41] Zhang Gao-Long, Liu Hao, and Le Xiao-Yun, Chin. Phys. B **18**, 136 (2009)
[42] D. T. Khoa, G. R. Satchler, and W. von Oertzen, Phys. Rev. C **56**, 954 (1997)

[43] R. A. N. Oliveira, N. Carlin, R. Liguori Neto *et al*., Nucl. Phys. A **856**, 46 (2011)
[44] L. C. Chamon *et al*., Phys. Rev. C **66**, 014610 (2002)
[45] N. M. Clarke (unpublished)
[46] E. D. Cooper, S. Hama, B. C. Clark *et al*., Phys. Rev. C **47**, 297 (1993)
[47] M. El-Azab Farid, Phys. Rev. C **74**, 064616 (2006)
[48] S. A. Fayans, O. M. Knyazkov, I. N. Kuchtin *et al*., Phys. Lett. B **357**, 509 (1995)
[49] I. Tanihata *et al*., Phys. Lett. B **287**, 307 (1992)
[50] M. V. Zhukov, Phys. Rep **231**, 151 (1993)
[51] M. Y. M. Hassan, M. Y. H. Farag, E. H. Esmael *et al*., Phys. Rev. C **79**, 014612 (2009)
[52] K. Yabana, Y. Ogawa, and Y. Suzuki, Phys. Rev. C **45**, 2909 (1992)
[53] F. Carstoiu and M. Lassaut, Nucl. Phys. A **597**, 269 (1996)
[54] J. S. Al-Khalili, Nucl. Phys. A **581**, 315 (1995)
[55] A. C. C. Villari *et al*., Phys. Phys. Lett. B **268**, 345 (1991)
[56] S. Shimoura, Proc. Second Int. Conf. on Radioactive Nuclear Beams, Louvain-La-Neuve, 1991, ed. Th. Delbar, p. 215 (Hilger, Bristol, 1992)
[57] B. Blank *et al*., Nucl. Phys. A **555**, 408 (1993)
[58] M. A. Hassanain, M. Anwar, and Kasem O. Behairy, Phys. Rev. C **97**, 044610 (2018)
[59] M. A. Hassanain *et al*., Phys. Rev. C **98**, 014621 (2018)
[60] Zakaria M. M. Mahmoud, A. Hemmdan, and Kassem O. Behairy, Results in Phys. **16**, 102892 (2020)